RESEARCH PAPER

Diosmetin-Assisted Green Synthesis of Zinc Oxide Nanoparticles and Development of a Nanogel for Enhanced Wound-Healing Activity

Sathiyavani.G[1*] , Dr. Akilandeswari.S[2]

[1*]Research Scholar, School of Pharmacy, Dhanalakshmi Srinivasan University, Samayapuram, Trichy, Tamil Nadu, India. E.mail address: sathiyavani1707@gmail.com

[2]Dean and Professor, School of Pharmacy, Dhanalakshmi Srinivasan University, Samayapuram, Trichy, Tamil Nadu, India. E.mail address: dean.pharmacy@dsuniversity.ac.in

Abstract

Aim

The present study was designed to biosynthesise ZnO nanoparticles using diosmetin, an active constituent from Clinacanthus nutans extract, incorporate the nanoparticles into nanogel formulations, and investigate their physicochemical properties along with their wound-healing efficacy.

Materials & Methods

ZnO nanoparticles were prepared by a microwave-assisted green synthesis method using diosmetin which was isolated from Clinacanthus nutans extract and characterised. The synthesised nanoparticles were analysed using various spectroscopic techniques. The synthesised ZnO NPs were then incorporated into Carbopol 934-based nanogels (F1–F5) with varying polymer concentrations. The optimised formulation was assessed for pH, viscosity, spreadability, cytocompatibility by MTT assay, and cell migration by scratch assay using the 3T3-L1 cell line.

Results

The synthesis of ZnO NPs was confirmed by a colour change, and their characteristic features were evaluated by spectroscopic and structural analyses. XRD revealed a highly crystalline hexagonal wurtzite phase, while SEM showed irregular and agglomerated nanoparticles. Among the nanogel formulations, F4 showed the most desirable balance of pH, viscosity, and spreadability, making it the optimised formulation. The ZnO-based nanogel was cytocompatible at lower concentrations with an IC50 of 69.74 µg/mL and enhanced cell migration in the scratch assay with wound closure of 63% at 35 µg/mL and nearly 69% at 70 µg/mL, indicating its wound-healing potential.

Conclusion

Diosmetin-based ZnO nanogel, particularly formulation F4, demonstrated promising physicochemical and biological properties for topical wound-healing applications.

Keywords: Clinacanthus nutans, nanogel, wound healing, cell migration, diosmetin.

How to cite this article: Sathiyavani.G Akilandeswari.S. Diosmetin-Assisted Green Synthesis of Zinc Oxide Nanoparticles and Development of a Nanogel for Enhanced Wound-Healing Activity. Int J Drug Deliv Technol. 2026;16(79s):1288-1291. DOI: 10.25258/ijddt.16.79s.210.

GRAPHICAL

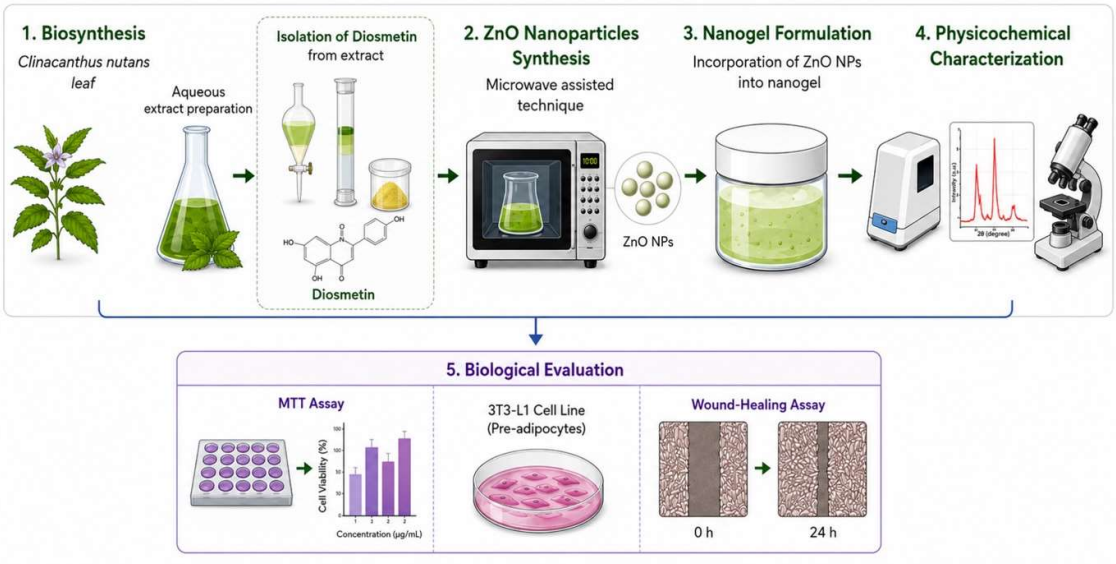

1. Introduction

The human skin, the largest organ, forms a protective barrier between the internal environment and external surroundings. It supports moisturization, thermoregulation, sensory perception, humoral equilibrium, and defense against pathogens. Damage or breakdown of healthy skin, due to various external factors, results in the formation of a wound. This causes pain and discomfort, and severe cases lead to disability. Wounds are categorised as acute or chronic. Acute wounds, due to surgical incisions or bites, usually heal

through predictable processes without external intervention within 8 to 12 weeks. Chronic wounds do not heal within 12 weeks or recur, often because acute trauma was untreated. Those associated with diabetes and vascular disorders are difficult to treat because of complex pathological mechanisms, prolonged inflammation, insufficient angiogenesis, and severe complications. Effective management requires moisture balance, targeted therapeutic agents to stimulate regeneration, and infection prevention through protective barriers against external contaminants (Das et al., 2025; Tayebi-Khorrami et al., 2025).

Wound dressings are broadly classified into two categories: traditional method, which includes bandages, gauze, etc., whereas modern dressings encompass hydrogels, nanofibers, scaffolds, etc. A major limitation of traditional dressings is that their removal often causes pain and tissue damage. In contrast, modern dressings, particularly hydrogels, help minimise these issues due to their distinctive physicochemical properties, thereby promoting faster healing. Hydrogels are three-dimensional network structures capable of retaining up to 95% water, providing a scaffold-like environment that supports enhanced cell proliferation and accelerates wound healing due to their distinctive properties. It exhibits excellent elasticity, flexibility, and swelling capacity and offers a cooling effect at the wound site, which significantly alleviates patient discomfort and pain (Valipour et al., 2023). In recent days, nanoparticles have gained attention in wound treatment due to their high surface area, size and targeted delivery, thereby enhancing therapeutic effect and low rate of adverse events.

Nanogels are nanoscale, hydrogel-based particles composed of crosslinked polymer networks that can absorb substantial amounts of water while maintaining structural integrity. Derived from natural, synthetic, or hybrid polymers, they exhibit tunable properties such as size, porosity, and degradability, enabling efficient loading of diverse therapeutic agents, including drugs, proteins, etc. Their high swelling capacity and hydrophilic nature support stability and effective biological interaction. It also enables controlled and targeted drug delivery by protecting encapsulated cargo and releasing it in response to stimuli such as pH, temperature, or enzymes, ensuring site-specific action. In wound healing, this facilitates localised delivery of bioactive molecules such as growth factors, antibiotics, and nanoparticles, promoting cell proliferation, angiogenesis, and tissue regeneration while reducing infection and improving therapeutic outcomes (Das et al., 2025; Zafaryab & Vig, 2025).

Zinc is an essential micronutrient that supports skin integrity by regulating wound healing processes, gene expression, and DNA repair. Zinc oxide nanoparticles (ZnO NPs) possess antibacterial, angiogenic activity, cell proliferation, and removal of necrotic tissue, thereby accelerating tissue repair and reducing infection risk. Increasingly, green synthesis approaches using plant extracts and other biological systems are being adopted to produce ZnO NPs in an eco-friendly and scalable manner, enhancing their functionality, antioxidant potential, and antimicrobial efficiency. Incorporation of such biogenically synthesised nanoparticles into wound dressings, including hydrogels and scaffolds, represents a promising strategy for developing safe, sustainable, and effective wound healing systems (S. N. Nandhini et al., 2023; Xiao et al., 2025).

Clinacanthus nutans, a widely used medicinal herb in Southeast Asia, has been traditionally employed for treating conditions such as skin infections, burns, diabetes, and snake bites. Its extracts are rich in bioactive compounds, including flavonoids, triterpenoids, steroids, phytosterols, and glycosides. Experimental studies have validated several pharmacological properties of C. nutans, including anti-inflammatory, antioxidant, antimicrobial, antiviral, anticancer, antidiabetic, immunomodulatory, and wound healing activities. Moreover, it enhances fibroblast migration and wound closure potential, indicating promise for tissue repair applications (Khoo et al., 2018).

The present work describes the microwave-assisted green synthesis of zinc oxide nanoparticles (ZnO NPs) employing diosmetin, an active constituent from Clinacanthus nutans extract, followed by comprehensive physicochemical characterisation. The synthesised nanoparticles were subsequently incorporated into a nanogel system, and key formulation parameters were evaluated to assess their stability and suitability for biomedical applications. The biocompatibility of the developed system was examined through MTT-based cytotoxicity analysis, while its therapeutic potential was further investigated using an in vitro wound healing assay in 3T3 cell lines. Together, these approaches aim to establish an effective, plant-mediated nanoplatform for enhanced wound healing applications.

2Materials & Methods

2.1Materials Used

Zinc acetate dihydrate (ACS reagent, ≥99.0%), sodium hydroxide (analytical grade), dimethyl sulfoxide (DMSO), diosmetin and Carbopol 934 (NF polymer) were obtained from Sigma-Aldrich and employed without further purification.

2.2Preparation of Extract

Fresh Leaves and stems of Clinacanthus nutans was collected from Palayamkottai region. It was washed thoroughly in distilled water and subsequently shade-dried. The dried parts were then ground into fine powder. Plant powder (10g) was dissolved in 100 mL of water, added, and then heated to 60°C for 15 minutes.

2.3Isolation of Active Constituents

2.3.1Column Chromatography

Column chromatographic separations were performed using silica gel (50–200 mesh, Merck). The plant extract was dissolved in methanol and adsorbed onto silica gel (60–120 mesh). The dried, adsorbed material was subsequently loaded onto a silica gel column (100–200 mesh) pre-packed with petroleum ether. The column was initially eluted with petroleum ether, followed by a gradient elution using petroleum ether–ethyl acetate mixtures of gradually increasing polarity (90:10, 80:20, 70:30, 60:40, 50:50, 40:60, 30:70, 20:80, and 10:90, v/v), and finally with 100% ethyl acetate. The column was then eluted with ethyl acetate–chloroform mixtures (90:10, 80:20, 70:30, 60:40, 50:50, 30:70, and 20:80, v/v), followed by 100% chloroform. Further elution was

performed using chloroform–methanol mixtures with increasing polarity (99:1, 98:2, 97:3, 96:4, 95:5, 94:6, 92:8, 90:10, 88:12, 85:15, and 80:20, v/v), followed by 100% methanol.

2.3.2Thin Layer Chromatography

The fractions were collected and analysed by thin-layer chromatography (TLC) on silica gel 60 PF_{254} plates to monitor the collected fractions and assess the purity of the isolated compounds. The fractions which exhibits a single spot were collected and then concentrated under reduced pressure to yield a crude solid. The crude material was further purified by treatment with activated charcoal in hot ethanol, followed by filtration. The resulting filtrate was allowed to cool and crystallise, affording the purified compound as a solid. The isolated compound was subsequently characterised by mass spectrometry, 1H-NMR, and 13C-NMR spectroscopy for structural elucidation.

2.4Identification and Characterisation of Active Constituents

The melting points of the isolated compounds were determined in open-ended glass capillary tubes using a SERVO melting point apparatus. FT-IR spectra were recorded as KBr pellets using a Bruker alpha-II spectrophotometer. The 1H and 13C NMR spectra were recorded on a JEOL 400 MHz NMR spectrometer using DMSO-d_6 as the solvent. Mass spectra were acquired using a JEOL AccuTOF JMS-T100 LC mass spectrometer.

2.5Preparation of Nanoparticle

A 200 mM zinc acetate solution was mixed with 5 mL of diosmetin dissolved in DMSO under constant stirring (1000 rpm), followed by the dropwise addition of 0.5 M NaOH at room temperature until a light-brown $Zn(OH)_2$ precipitate was formed. The reaction mixture was subjected to microwave irradiation (800 W, 5 min) to convert the precipitate into ZnO nanoparticles. The nanoparticles were recovered by centrifugation at 3900 rpm for 30 min, washed repeatedly with distilled water and ethanol, dried at 60 °C for 24 h, and stored in an airtight container for subsequent analyses (Alharthi et al., 2021).

2.6Characterization

2.6.1UV–Vis spectroscopy analysis

The optical behaviour of the isolated active constituent of Clinacanthus nutans extract and biosynthesised ZnO nanoparticles was investigated by UV–Visible spectroscopy using a spectrophotometer (Shimadzu Corporation, Japan). Absorbance spectra were acquired within the wavelength range of 200–800 nm. For nanoparticle characterisation, 0.05 g of ZnO nanoparticles was dispersed in 5 mL of 96% ethanol, and the resulting suspension was analysed over the same spectral range.

2.6.2DLS Analysis

The average hydrodynamic diameter and particle size distribution of the synthesised ZnO nanoparticles were evaluated by dynamic light scattering (DLS) using a Zetasizer V2.2 (Malvern Instruments, Worcestershire, UK). In addition, the zeta potential was measured with water as the dispersing medium to evaluate the stability of the nanoparticles.

2.6.3XRD Analysis

The structural and crystalline properties of the synthesised ZnO nanoparticles were evaluated by X-ray diffraction (XRD) using an X'Pert Analytical diffractometer with an operating voltage of 40 kV and a current of 30 mA. X-ray diffraction patterns were recorded over a 2θ range of 20°–80° using Cu Kα radiation with a wavelength of 1.541 Å.

2.6.4FTIR Analysis

Fourier-transform infrared (FTIR) spectroscopy was used to characterise the phytochemical functional groups of the isolated active constituent of Clinacanthus nutans extract and biosynthesised ZnO nanoparticles. FTIR spectra were recorded using a Nicolet 6700 spectrometer (Shimadzu Corporation, Kyoto, Japan) over a wavenumber range of 400–4000 cm^{-1} to identify biomolecules responsible for nanoparticle reduction and stabilisation.

2.6.5SEM Analysis

Scanning electron microscopy (SEM) (JEOL JSM-6390) was employed to evaluate the morphological features and surface architecture of the synthesised ZnO nanoparticles at a temperature of 25±2 oC.

2.7Nanogel Formulation

Five gel formulations (F1–F5) containing different concentrations of Carbopol 934 (40, 50, 60, 70, and 80 mg) were prepared by dispersing the polymer in 20 mL of distilled water. The dispersions were magnetically stirred at room temperature for 1–1.5 h to ensure complete hydration and the formation of homogeneous gels. 20 mg of ZnO nanoparticles were dispersed in 1–1.5 mL of distilled water and then gradually incorporated into each formulation of Carbopol dispersion under constant stirring. The mixture was further homogenised using probe sonication at an amplitude of 90 for 90 cycles to ensure even distribution of the nanoparticles within the gel matrix. Finally, gelation was achieved by the dropwise addition of 10% NaOH solution to neutralise the formulation (Hassan et al., 2023).

2.8Physiochemical Evaluation

The five different formulations of nanogel were evaluated for morphological characteristics, including colour, appearance, and homogeneity, through visual inspection. The pH of each nanogel formulation was measured using a calibrated digital pH meter (Mettler Toledo, Japan) at 25±2 oC. For this, 1 g of gel was dispersed in 100 mL of double-distilled water and allowed to equilibrate for 2 hours, after which the pH electrode was immersed in the sample to record the value. The spreadability was evaluated following standard procedures. For spreadability assessment, a 1g gel was placed between two glass slides and compressed with a 100 g weight to form a uniform thin film. The upper slide was then allowed to move under a 20 g load, and the time required to travel a distance of 7.5 cm was recorded to calculate spreadability. The viscosity was determined using a Brookfield viscosity monitor (Alam et al., 2022).

2.9MTT Assay

The cytocompatibility of the formulated DNZnO nanogel was assessed by the MTT colorimetric assay using the 3T3-L1 mouse fibroblast cell line (Perumal et al., 2024). Cells procured from the National Centre for Cell Science (NCCS, Pune, India) were maintained in Dulbecco's

Modified Eagle Medium (DMEM) supplemented with 10% fetal bovine serum (FBS) and 1% antibiotic–antimycotic solution under a humidified atmosphere containing 5% CO_2 at 37 °C. For the assay, cells were dispensed into 96-well culture plates at a density of 5 × 10^3–1 × 10^4 cells per well in 100 µL of complete growth medium and incubated for 24 h to permit cell attachment. Following incubation, the culture medium was replaced with fresh medium containing DNZnO nanogel at concentrations ranging from 6.25 to 100 µg/mL, whereas untreated cells were maintained as the control. After a 24 h exposure period, 10 µL of MTT reagent (5 mg/mL prepared in phosphate-buffered saline) was added to each well, and the plates were further incubated for 3–4 h to allow intracellular reduction of MTT into insoluble formazan crystals by metabolically active cells. The culture medium was then carefully aspirated, and 100 µL of dimethyl sulfoxide (DMSO) was added to each well to dissolve the formazan crystals. The plates were gently agitated until complete solubilization was achieved, and absorbance was measured at 570 nm using a microplate reader. All treatments were performed in triplicate, and the results are expressed as mean ± standard deviation (SD). The half-maximal inhibitory concentration (IC_{50}) of the DNZnO nanogel was calculated by fitting a nonlinear dose–response curve using GraphPad Prism software.

2.10Scratch Assay

An in vitro scratch wound assay was performed to investigate the effect of the DNZnO nanogel on fibroblast migration. Briefly, 3T3-L1 mouse fibroblast cells were cultured in 6-well plates at a density of 3–5 × 10^5 cells per well until a confluent monolayer (90–100%) was obtained. A uniform linear scratch was generated using a sterile 200 µL pipette tip to create an artificial wound. Following removal of detached cells by washing with phosphate-buffered saline (PBS), serum-free medium containing DNZnO nanogel at 35 or 70 µg/mL (corresponding to the IC_{25} and IC_{50} concentrations) was added. Untreated cells maintained under identical conditions served as the control. Microscopic images of the wounded area were captured at 0 and 48 h using an inverted phase-contrast microscope. Cell migration was quantified by measuring the reduction in wound area with ImageJ software, and the percentage of wound closure was calculated relative to the initial wound area (J. Nandhini et al., 2025).

2.11Statistical Analysis

Statistical analysis was performed using GraphPad Prism 9.0, while ImageJ was used for image-based quantitative measurements. Data are expressed as mean ± standard deviation (SD), and error bars indicate the corresponding standard deviation.

3Results

3.1Isolation of Active Constituents

A total of 49 fractions were collected, among which fractions 22–29 exhibited a single
spot with an identical Rf value of 0.64, suggesting the presence of a homogeneous compound. The concentrated fraction of these combined fractions yielded a crude solid compound, which, upon purification, resulted in a yellow solid compound.

3.2Identification and Characterisation of Diosmetin

The isolated compound was obtained as a pale yellow solid with a melting point of 259–261 °C, indicating its high purity and crystalline nature. The molecular formula was determined to be $C_{16}H_{12}O_6$, corresponding to a molecular weight of 300.26 g/mol. Electrospray ionisation mass spectrometry (ESI-MS) analysis exhibited a prominent molecular ion peak at m/z 301.13 ($[M + H]^+$).

1H-NMR (DMSO-d6): δ ppm: 12.93 (s, 1H, -OH); 10.85 (s, 1H, -OH); 9.45 (s, 1H, -OH); 7.53 – 7.56 (dd, 1H, Ar-H); 7.42 – 7.43 (d, 1H, Ar-H); 7.07 – 7.10 (d, 1H, Ar-H); 6.75 (s, 1H, =CH); 6.46 (d, 1H, Ar-H); 6.19 – 6.20 (d, 1H, Ar-H); 3.86 (s, 3H, -OCH3).

13C-NMR (DMSO-d6): 191.16 (C4); 173.73 (C2); 172.98 (C7); 170.95 (C5); 166.79 (C9); 160.60 (C4'); 156.26 (C3'); 132.49 (C1'); 128.17 (C6'); 122.43 (C2'); 121.60 (C5'); 113.21 (C10); 112.99 (C3); 108.36 (C6); 103.38 (C8); 65.22 (-OCH3).

From these analyses, the flavonoid compound which is an oxygenated, methoxylated aromatic phenolic compound containing hydroxyl and carbonyl functionalities, is confirmed to be diosmetin.

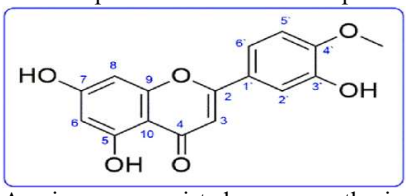

Figure 1 Structure of diosmetin

3.3Synthesis of ZnO nanoparticle

A microwave-assisted green synthesis strategy enabled the successful production of zinc oxide nanoparticles (ZnO NPs) using diosmetin, an active constituent isolated from Clinacanthus nutans extract. Upon microwave irradiation (800 W, 5 min), the reaction mixture transformed from light-brown to white, indicating the formation of ZnO NPs through the conversion of zinc hydroxide precipitate (Figure 1).

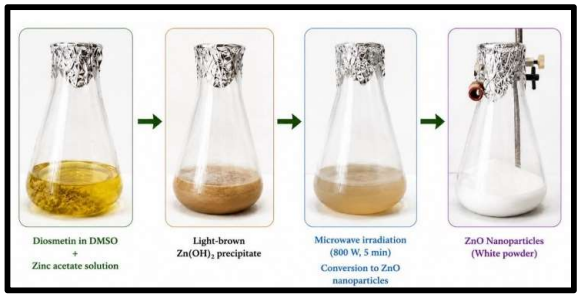

Figure 2 Green synthesis of zinc oxide nanoparticles using diosmetin

3.4Characterization

3.4.1UV-Visible Spectral analysis

The UV–Visible spectroscopy analysis of the isolated diosmetin, an active constituent isolated from Clinacanthus nutans extract and biosynthesised ZnO nanoparticles, is given in Figure 3. The UV–visible spectrum of diosmetin in ethanol exhibited a dominant absorption band between 320 and 390 nm, with a broad maximum in this region. The absorbance increased sharply from approximately 320 nm, reached a plateau with a pronounced peak in the mid-UV range, and declined rapidly beyond 390–400 nm. This behaviour is consistent with the typical flavone pattern, in which the principal Band I lies in the 300–380 nm region and reflects π→π* transitions in the cinnamoyl system of the B-ring.

In the case of ZnO nanoparticles, a distinct absorption peak near 350–380 nm, characteristic of the surface plasmon resonance (SPR) phenomenon. This absorption in the UV region confirms the successful formation of nanosized ZnO particles exhibiting excitonic absorption related to their intrinsic band gap transition. The sharpness and position of the SPR peak indicate the crystalline nature and uniform size distribution of the nanoparticles, which are critical for their optical and biomedical applications.

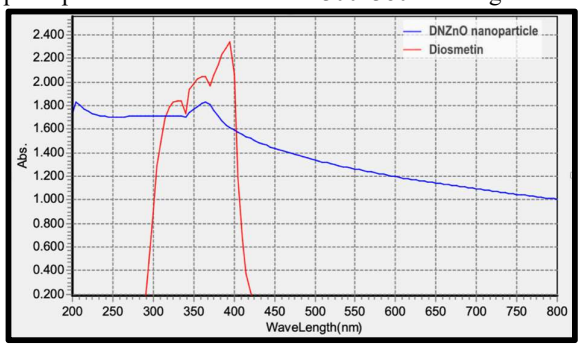

Figure 3 UV-Visible absorption spectra of Diosmetin and synthesised ZnO nanoparticles

3.4.2DLS

The hydrodynamic size of the synthesised ZnO nanoparticles was determined by DLS, yielding a Z-average diameter of 564.1 nm and a PDI of 0.776. The relatively high PDI value suggests considerable particle size heterogeneity and polydispersity. The electrophoretic light scattering (ELS) analysis revealed that mean zeta potential was measured at -16.31 mV, suggesting moderate colloidal stability due to the surface-bound phytochemicals contributing to electrostatic repulsion (Figure 3a and 3b). These results imply that the nanoparticles exhibit surface charge conducive to dispersion stability, and the relatively high PDI indicates a heterogeneous population.

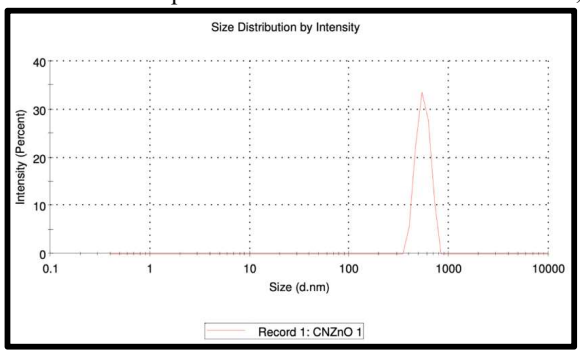

b)

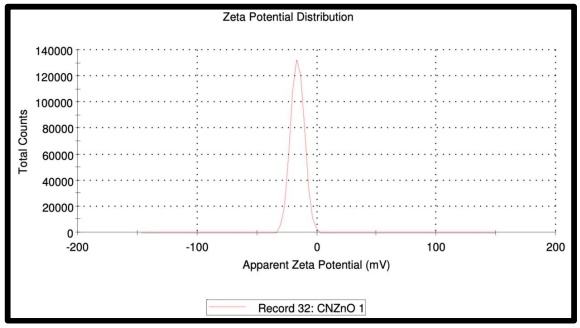

Figure 4 a) Particle size distribution and b) zeta potential of ZnO nanoparticles synthesised using diosmetin

3.4.3FTIR

The FT-IR spectrum of diosmetin exhibited a broad absorption band at 3536–3392 cm^{-1}, corresponding to the O–H stretching vibration of phenolic hydroxyl groups. The band at 3093 cm^{-1} was assigned to aromatic C–H stretching, while the strong absorption at 1650 cm^{-1} confirmed the presence of the conjugated carbonyl (C=O) group characteristic of the flavone backbone. Bands at 1610, 1583, 1502, and 1455 cm^{-1} were attributed to aromatic C=C skeletal vibrations, whereas the absorptions at 1438, 1361, 1255, 1164, and 1032 cm^{-1} corresponded to C–H bending and C–O stretching vibrations. The peaks at 944, 871, 809, 652, and 644 cm^{-1} were assigned to out-of-plane aromatic C–H bending, further confirming the characteristic functional groups of diosmetin.

The biosynthesised ZnO nanoparticle shows bands at 3392.24 cm^{-1} (stretching of O-H), 2365.57 and 2335.78 cm^{-1} (stretching of C=O). The stretching of the C-O functional group or the bending of C=C was shown by the presence of peaks at 1455.64 and 871.38 cm^{-1}, and notably at 651.92 cm^{-1}, which is attributed to Zn–O stretching vibrations, confirming the formation of ZnO nanoparticles (Figure 5). The retention of several absorption bands in the ZnO spectrum suggests the presence of phytochemical residues on the nanoparticle surface, indicative of their role in reduction and stabilisation during synthesis by acting as capping and stabilising agents.

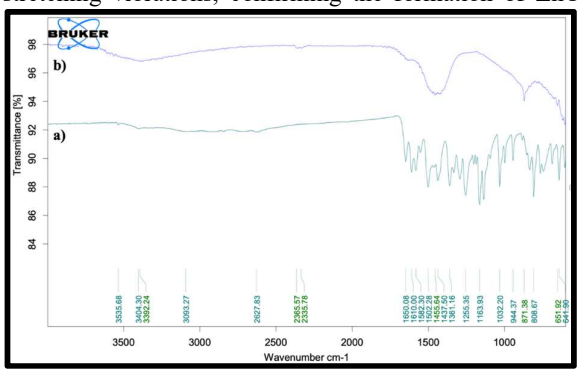

Figure 5 FTIR spectrum of a) diosmetin and b) ZnO nanoparticles synthesised using diosmetin

3.4.4XRD

The XRD pattern of the biosynthesized ZnO nanoparticles showed a series of intense diffraction peaks at 2θ values of approximately 31.8°, 34.5°, 36.3°, 47.6°, 56.7°, 62.9°, 66.5°, 68.0°, and 69.1° (Figure 6). These peaks were indexed to the (100), (002), (101), (102), (110), (103), (200), (112), and (201) lattice planes of the hexagonal wurtzite phase of ZnO (Figure 6),

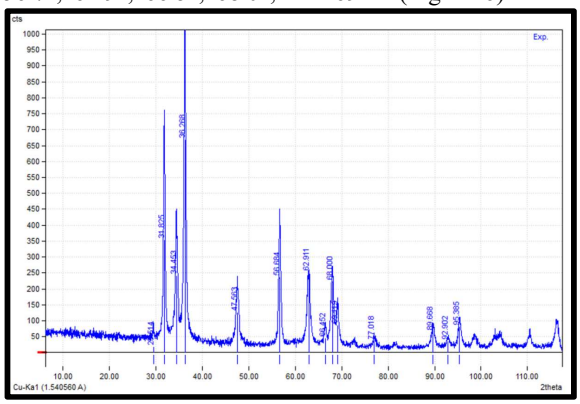

Figure 6 XRD pattern of ZnO nanoparticles synthesised using diosmetin

3.4.5SEM

The SEM imaging examined the surface morphology of the green-synthesised ZnO nanoparticles (Figure 7). The images show that nanoparticles appear to be irregular and highly agglomerated (closely packed), which is due to the presence of phytoconstituents on the surface as a capping agent.

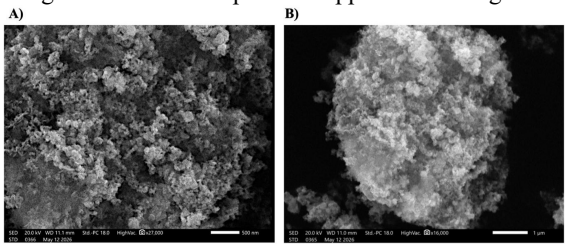

Figure 7 SEM image of ZnO Nanoparticles synthesised using diosmetin A) High magnification B) Low magnification

3.5Nanogel

Five ZnO nanoparticle-loaded nanogel formulations (F1–F5) were prepared using varying concentrations of Carbopol 934 as the gelling agent and ZnO nanoparticles as the active component (Table 1). The concentration of ZnO nanoparticles (20 mg) and neutralising agent (0.3 mL of 10% NaOH) was maintained constant in all formulations, while the Carbopol 934 concentration was varied from 40 to 80 mg to evaluate its effect on gel characteristics.

Table 1 Composition of ZnO nanoparticle-loaded nanogel formulations (F1–F5)

S. No	Formulation	Carbopol 934	ZnONPs	10% NaOH
	F1	40mg	20mg	0.3 ml
	F2	50mg	20mg	0.3 ml

	F3	60mg	20mg	0.3 ml
	F4	70mg	20mg	0.3 ml
	F5	80mg	20mg	0.3 ml

All ZnO nanoparticle-loaded nanogel formulations (F1–F5) exhibited a consistent cream-colored, semi-transparent appearance, reflecting uniformity in their general visual characteristics across batches (Table 2). However, notable variations were observed in their physicochemical properties, including consistency, pH, viscosity, and spreadability, attributable to differences in formulation composition.

The pH values ranged from 5.47 ± 0.03 to 6.86 ± 0.05, indicating overall compatibility with topical application. Among these, formulation F4 demonstrated a pH of 6.86 ± 0.05, aligning most closely with the physiological pH range suitable for skin, thereby suggesting enhanced biocompatibility. Rheological analysis revealed a progressive increase in viscosity from F1 (8,250 ± 95 cP) to F5 (17,320 ± 150 cP), indicating a corresponding enhancement in formulation thickness and structural firmness. Despite F5 exhibiting the highest viscosity, its significantly diminished spreadability (5.21 ± 0.08 g·cm/s) implies reduced ease of application. Conversely, F1 showed the greatest spreadability (7.85 ± 0.12 g·cm/s) but the lowest viscosity, which may negatively impact retention at the application site.

Formulation F4 emerged as the optimal balance between these parameters, with a viscosity of 14,870 ± 135 cP and spreadability of 6.83 ± 0.09 g·cm/s. It was characterized by a thick, homogeneous texture, indicating superior structural integrity and uniformity relative to other formulations. These attributes suggest that F4 combines adequate viscosity to enhance residence time with sufficient spreadability to facilitate convenient topical application. Collectively considering appearance, consistency, pH, viscosity, and spreadability, formulation F4 was identified as the optimized candidate. Its superior homogeneity, favourable rheological profile, and physiologically compatible pH underscore its suitability for further characterisation and biological evaluation.

Table 2 Comparative physicochemical properties of ZnO nanoparticle-incorporated nanogel formulations (F1–F5)

Formulation	Color	Appearance	Consistency	pH	Viscosity (cP)	Spreadability (g·cm/s)
F1	Cream-colored	Semi-transparent	Slightly viscous	5.47 ± 0.03	8,250 ± 95	7.85 ± 0.12
F2	Cream-colored	Semi-transparent	Moderately viscous	5.82 ± 0.04	10,140 ± 110	7.12 ± 0.10
F3	Cream-colored	Semi-transparent	Smooth and moderately thick	6.13 ± 0.03	12,460 ± 125	6.48 ± 0.11
F4	Cream-colored	Semi-transparent	Thick and homogeneous	6.86 ± 0.05	14,870 ± 135	6.83 ± 0.09
F5	Cream-colored	Semi-transparent	Highly viscous and firm	6.01 ± 0.04	17,320 ± 150	5.21 ± 0.08

3.5.1MTT Assay

The cytocompatibility profile obtained from the MTT assay demonstrated that the DNZnO (Diosmetin-zinc oxide nanoparticle) nanogel induced a dose-dependent decrease in the viability of 3T3-L1 fibroblast cells (Figure 8 and 9). Cell viability remained above 93% at concentrations of 6.25 and 12.5 µg/mL, indicating cytocompatibility. At 25 µg/mL, viability declined to approximately 81%, further decreasing to 63–66% at 50 µg/mL. The highest concentration, 100 µg/mL, resulted in a significant reduction in viability to 32–38%. The graph plotted with the concentration of the DNZnO-based nanogel and the percentage of cell viability. The IC_{50} value was calculated to be 69.74 µg/mL, reflecting the concentration at which half of the cells remained viable.

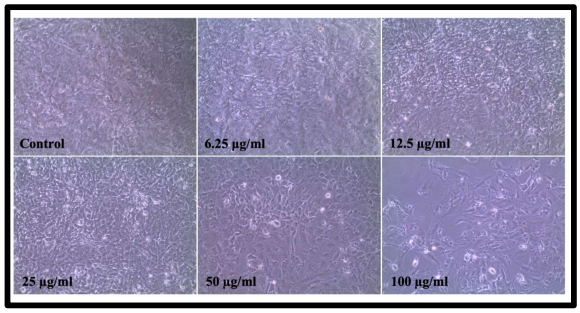

Figure 8 MTT assay of DNZnO nanogel

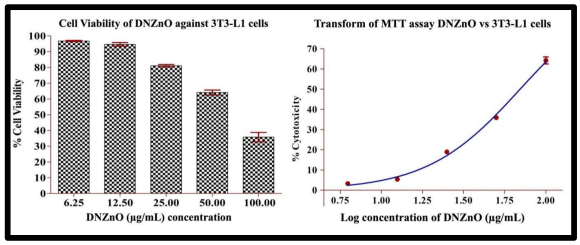

Figure 9 MTT assay showing the cytocompatibility of DNZnO nanogel in 3T3-L1 fibroblast cells (A) Cell viability at different concentrations. (B) Concentration-dependent cytotoxicity curve used to estimate the IC_{50} value (69.74 µg/mL). Values are expressed as mean ± SD (n = 3)

3.5.2Scratch Assay

The scratch assay results demonstrated that DNZnO-based nanogel significantly promoted 3T3-L1 cell migration and wound closure compared to the untreated control group (Figure 10 and 11). After 48 hours, the control group exhibited only partial wound closure, whereas treatment with DNZnO-based nanogel at IC25 and IC50 concentrations of 35 µg/mL and 70 µg/mL resulted in a reduction in wound area, with the higher concentration. Quantitative analysis revealed that wound closure increased from approximately 55% in the control group to about 63% at 35 µg/mL and nearly 69% at 70 µg/mL, indicating a concentration-dependent upregulation of cell migration and wound healing.

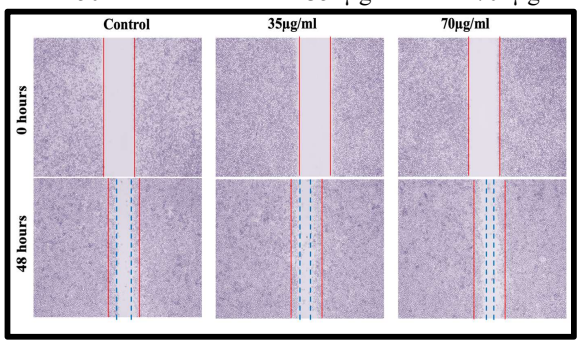

Figure 10 Effect of DNZnO on 3T3-L1 cell migration

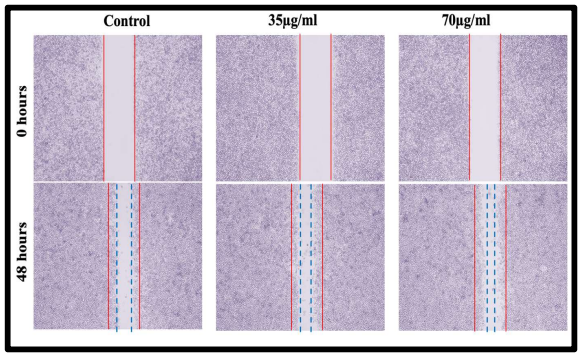

Figure 11 Wound-healing activity of DNZnO nanogel in 3T3-L1 fibroblast cells determined by scratch assay

4. Discussion

Zinc oxide (ZnO) nanoparticles have emerged as promising agents in wound care owing to their potent antimicrobial and anti-inflammatory properties. They facilitate cell proliferation and enhancing tissue regeneration, while maintaining biocompatibility and safety. Incorporation of ZnO nanoparticles into wound dressings or topical formulations has been shown to accelerate wound closure and reduce microbial colonization, thereby improving healing outcomes. Moreover, ZnO nanoparticles may act synergistically with other therapeutic agents, offering a multifaceted approach to managing wounds (Lababidi et al., 2026; Usmaev et al., 2024). This innovative strategy holds potential advantages over conventional treatments, although further clinical research is necessary to fully realise their application in practice.

Clinacanthus nutans extract has already been reported to consist of numerous phytochemicals – flavonoids, tannins, alkaloids, saponins, etc. (Yusuf et al., 2020). The active constituent that was isolated from the extract was diosmetin.

The spectral data of diosmetin indicate the presence of a highly oxygenated aromatic compound. The ^{1}H-NMR spectrum (DMSO-d_6) showed three downfield singlets at δ 12.93, 10.85, and 9.45 ppm, attributable to three hydroxyl protons, with the strongly deshielded signal at δ 12.93 ppm suggesting a hydrogen-bonded phenolic hydroxyl group. The aromatic proton signals observed at δ 7.53–7.56 (dd), 7.42–7.43 (d), 7.07–7.10 (d), 6.46 (d), and 6.19–6.20 (d) ppm indicated the presence of aromatic rings with different substitution patterns. A singlet at δ 6.75 ppm (1H) was assigned to an olefinic (=CH) proton, while the singlet at δ 3.86 ppm (3H) was characteristic of a methoxy (–OCH_3) group. The ^{13}C-NMR spectrum displayed signals at δ 191.16 ppm corresponding to a carbonyl carbon (C-4), together with oxygenated and conjugated carbon signals in the region of δ 160.60–103.38 ppm, supporting the presence of phenolic and aromatic carbons. The signal at δ 65.22 ppm was assigned to the methoxy carbon. The slight bathochromic displacement of Band I toward the upper end of the 300–380 nm interval can be attributed to the electron-donating substituents on the flavone skeleton, notably the methoxy group at C-4′ and hydroxyl groups at C-5 and C-7. Such substituents are known to modulate both wavelength and intensity of flavonoid absorption bands by altering electron density and conjugation across the aromatic rings. These data were found to be similar to published literature (Yan et al., 2020). Diosmetin when mixed with a zinc salt, Zn2+ ions will form complexes and then react

with the hydroxide ions from the phenolic group of the phytochemical, generating a zinc hydroxide precipitate, which is brown in color. When the precipitate is exposed to microwave radiation, interactions occur between the phytochemicals and metal ions, resulting in the conversion of zinc hydroxide to ZnO nanoparticles (Alharthi et al., 2021).

The peak in the UV-spectral analysis of diosmetin and synthesised ZnO nanoparticles is due to the oscillation of electrons in the conduction band at a specific wavelength and this aligns with the previous studies (Jain et al., 2020; Sheoran et al., 2023). The peak at 370 to 390 nm confirms the formation of ZnO nanoparticles, as this range is specific for metal oxide nanoparticles, and the broad peak indicates their polydispersity property (Perumal et al., 2024). FTIR analysis of the synthesised ZnO nanoparticles shows a peak at 651.92 cm^{-1}, which is specific for the metal oxides, and it aligns with the other studies (Thien et al., 2025). The retention of peaks in the higher wavenumber region suggests that phytochemicals from the extract remained adsorbed on the nanoparticle surface, providing stabilization and preventing aggregation (Kumari et al., 2024). This supports the role of C. nutans extract in the green synthesis by reduction and surface capping of ZnO nanoparticles.

The narrow size distribution of the synthesised ZnO nanoparticles observed by DLS suggests that the nanoparticles were well dispersed and that the plant-derived phytochemicals likely contributed to surface stabilisation during synthesis (Shiraz et al., 2024). The negative zeta potential value indicates that the nanoparticle surface carried a net negative charge, which may arise from adsorbed phytoconstituents containing hydroxyl, carboxyl, or phenolic groups. This surface charge facilitates electrostatic interactions that prevent particle agglomeration, thereby contributing to the stability of the nanoparticle suspension (Fouda et al., 2018). The presence of well-defined diffraction peaks confirms that the ZnO nanoparticles formed a crystalline hexagonal wurtzite structure. Each peak corresponds to the lattice (100), (002), (101), (102), (110), (103), (200), (112), (201), (004) and (202), which is in accordance with the (JCPDS card No: 36-1451) (Abdelbaky et al., 2022). SEM analysis shows that the synthesised nanoparticles appear as aggregated ones, which is due to the presence of capping agents from the extract on their surface to stabilise the nanoparticles. The physicochemical formulation of F4 is chosen to be the most suitable for the delivery of synthesised ZnO nanoparticles, which is due to its pH slightly near acidic, which reduces the irritation and maintains the compatibility barrier with the skin (Lukić et al., 2021). Moreover, the spread ability and viscosity of the formulation enhance the spreading and stability properties suitable for wound healing applications (Ghiorghita et al., 2024).

The MTT assay is a widely used method for evaluating the cytocompatibility of plant-mediated ZnO nanoparticles by quantifying mitochondrial metabolic activity as an indicator of viable cells. This assay provides critical insight into the biocompatibility of nanoparticles by quantifying the reduction of MTT to formazan by metabolically active cells. ZnO nanoparticles synthesized using diosmetin from Clinacanthus nutans extract exhibited favorable cytocompatibility due to the presence of phytochemicals that act as capping and stabilizing agents, reducing potential cytotoxic effects (Steffy et al., 2018).

The wound-healing potential of diosmetin-based ZnO nanoparticles may be attributed to the combined bioactive properties of both diosmetin and the nanoparticle platform. C. nutans extract is known to suppress key inflammatory mediators, thereby modulating inflammatory signaling and limiting the early amplification phase of the wound response. In addition, its cytoprotective effect on endothelial cells may support vascular integrity and improve the microenvironment required for tissue regeneration. These properties are particularly relevant in the early stages of wound repair, where controlled inflammation and endothelial survival are essential for successful healing (Limpanich et al., 2025). ZnO nanoparticles contribute well-established therapeutic effects, including antioxidant, anti-inflammatory, and antibacterial activities. These actions may help reduce oxidative stress, prevent infection-associated complications, and create a favourable environment for tissue repair. ZnO nanoparticles are also reported to enhance angiogenesis, cell migration, proliferation, collagen deposition, and extracellular matrix remodeling, all of which are critical events in wound closure and restoration of tissue architecture. Their ability to support glucose uptake further adds relevance for diabetic wound healing, where impaired repair is often associated with hyperglycemia and chronic inflammation (Xiao et al., 2025).

Taken together, the synergistic interaction between diosmetin and ZnO nanoparticles may provide a multifaceted mechanism for wound repair. Diosmetin may primarily contribute anti-inflammatory and cytoprotective effects, while ZnO nanoparticles may enhance antimicrobial defense, oxidative stress control, and regenerative processes. Taken together, these results demonstrate that diosmetin-based ZnO nanoparticles represent a promising candidate for topical wound-healing applications, particularly in wounds that exhibit persistent inflammation, increased susceptibility to infection, and decreased tissue regeneration.

5Limitation and Future Direction

Nevertheless, certain limitations of this study should be acknowledged. The present work focused on the green synthesis of ZnO nanoparticles using diosmetin from Clinacanthus nutans extract and the subsequent development of nanogel formulations with desirable physicochemical characteristics. Although the synthesized ZnO nanoparticles were evaluated for cytocompatibility and wound-healing potential, further in vitro and in vivo investigations are warranted to elucidate the underlying molecular and cellular mechanisms involved in their therapeutic action. Moreover, future studies should focus on the optimization of advanced nanogel-encapsulated formulations and a more comprehensive evaluation of their efficacy in wound healing models.

6Conclusion

The integration of green-synthesised ZnO nanoparticles using diosmetin from Clinacanthus nutans extract into a

Carbopol nanogel resulted in a stable and biocompatible wound-healing formulation with encouraging in vitro performance. The optimized F4 nanogel demonstrated suitable physicochemical characteristics, preserved cell viability, and accelerated fibroblast migration, indicating its potential to facilitate tissue repair. These results establish diosmetin -mediated ZnO nanogel as a promising biomaterial for wound management and support further mechanistic, in vivo, and translational studies toward clinical application.

Statements & Declarations

Funding

This research did not receive any specific grant from funding agencies in the public, commercial, or not-for-profit sectors.

Competing Interest

The authors declared that they have no known competing financial interests or personal relationships that could have appeared to influence the work reported in this paper. The authors have no conflict of interest.

Ethics approval

This study did not involve human participants, human data or human tissue, and no live animals were used at any stage. Consequently, formal ethical approval was not required for this study.

Consent to participate

This study did not involve human participants; therefore, informed consent is not applicable.

Consent to publish

This study does not contain any individual person's data in any form (including individual details, images, or videos).

Availability of data and materials

All data generated or analyzed during this study are included in this article. Detailed methodologies and data are presented within the main text.

Bibliographic References:

1. Abdelbaky, A. S., Abd El-Mageed, T. A., Babalghith, A. O., Selim, S., & Mohamed, A. M. H. A. (2022). Green Synthesis and Characterization of ZnO Nanoparticles Using Pelargonium odoratissimum (L.) Aqueous Leaf Extract and Their Antioxidant, Antibacterial and Anti-inflammatory Activities. Antioxidants, 11(8), 1444. https://doi.org/10.3390/ANTIOX11081444
2. Alam, A., Foudah, A. I., Salkini, M. A., Raish, M., & Sawale, J. (2022). Herbal Fennel Essential Oil Nanogel: Formulation, Characterization and Antibacterial Activity against Staphylococcus aureus. Gels, 8(11). https://doi.org/10.3390/gels8110736
3. Alharthi, M. N., Ismail, I., Bellucci, S., Khdary, N. H., & Abdel Salam, M. (2021). Biosynthesis microwave-assisted of zinc oxide nanoparticles with ziziphus jujuba leaves extract: Characterization and photocatalytic application. Nanomaterials, 11(7), 1682.
4. Das, T., Das, M., Sultana, S., & Swain, R. (2025a). Stimuli-responsive nanogels in wound care: A comprehensive review. Next Nanotechnology, 8, 100260.
5. Das, T., Das, M., Sultana, S., & Swain, R. (2025b). Stimuli-responsive nanogels in wound care: A comprehensive review. Next Nanotechnology, 8, 100260.
6. Fouda, A., Saad, E., Salem, S. S., & Shaheen, T. I. (2018). In-Vitro cytotoxicity, antibacterial, and UV protection properties of the biosynthesized Zinc oxide nanoparticles for medical textile applications. Microbial Pathogenesis, 125, 252–261.
7. Ghiorghita, C.-A., Platon, I.-V., Lazar, M. M., Dinu, M. V., & Aprotosoaie, A. C. (2024). Trends in polysaccharide-based hydrogels and their role in enhancing the bioavailability and bioactivity of phytocompounds. Carbohydrate Polymers, 334, 122033.
8. Hassan, R. R. A., Hassan, H. M., Mohamed, Y. A., Ismail, M. E. M., Farid, Y., Mohamed, H., Ismail, S. H., Salem, M. Z. M., & Abdel-Hamied, M. (2023). ZnO, TiO2 and Fe3O4/Carbopol hybrid nanogels for the cleaner process of paper manuscripts from dust stains and soil remains. Heritage Science, 11(1), 221. https://doi.org/10.1186/s40494-023-01063-7
9. Jain, D., Shivani, Bhojiya, A. A., Singh, H., Daima, H. K., Singh, M., Mohanty, S. R., Stephen, B. J., & Singh, A. (2020). Microbial Fabrication of Zinc Oxide Nanoparticles and Evaluation of Their Antimicrobial and Photocatalytic Properties. Frontiers in Chemistry, 8. https://doi.org/10.3389/fchem.2020.00778
10. Khoo, L. W., Audrey Kow, S., Lee, M. T., Tan, C. P., Shaari, K., Tham, C. L., & Abas, F. (2018). A comprehensive review on phytochemistry and pharmacological activities of Clinacanthus nutans (Burm. F.) Lindau. Evidence-Based Complementary and Alternative Medicine, 2018(1), 9276260.
11. Kumari, M., Sadhu, P., Talele, C., & Shah, N. (2024). Green nanotechnology: How plants can help synthesize nanoparticles for biomedical and environmental purposes. J. Nat. Remedies, 24, 1021–1034.
12. Lababidi, J. M., Ali, S., Shaheen, B., & Allam, N. K. (2026). Recent developments in zinc oxide-polymer nanocomposites for enhanced wound healing applications. Biomedical Materials, 21(1), 012008.
13. Limpanich, N., Chayapakdee, P., Mekawan, K., Thongyim, S., Yongsawas, R., Khamwong, P., Tragoolpua, Y., Kaewkod, T., Jangsutthivorawat, S., Jungklang, J., Chanasut, U., Inta, A., Arjinajarn, P., Panya, A., & Pandith, H. (2025). Integrative Wound-Healing Effects of Clinacanthus nutans Extract and Schaftoside Through Anti-Inflammatory, Endothelial-Protective, and Antiviral Mechanisms. International Journal of Molecular Sciences, 26(13), 6029. https://doi.org/10.3390/ijms26136029
14. Lukić, M., Pantelić, I., & Savić, S. D. (2021). Towards optimal ph of the skin and topical

formulations: From the current state of the art to tailored products. Cosmetics, 8(3), 69.

15. Nandhini, J., Karthikeyan, E., Sheela, M., Bellarmin, M., Gokula Kannan, B., Pavithra, A., Sowmya Sri, D., Siva Prakash, S., & Rajesh Kumar, S. (2025). Optimization of microwave-assisted green synthesis of zinc oxide nanoparticles using Ocimum americanum and Euphorbia hirta extracts: In vitro evaluation of antioxidant, anti-inflammatory, antibacterial, cytotoxicity, and wound healing properties. Intelligent Pharmacy, 3(1), 90–109. https://doi.org/10.1016/j.ipha.2024.09.003
16. Nandhini, S. N., Sisubalan, N., Vijayan, A., Karthikeyan, C., Gnanaraj, M., Gideon, D. A. M., Jebastin, T., Varaprasad, K., & Sadiku, R. (2023). Recent advances in green synthesized nanoparticles for bactericidal and wound healing applications. Heliyon, 9(2).
17. Perumal, P., Sathakkathulla, N. A., Kumaran, K., Ravikumar, R., Selvaraj, J. J., Nagendran, V., Gurusamy, M., Shaik, N., Gnanavadivel Prabhakaran, S., Suruli Palanichamy, V., Ganesan, V., Thiraviam, P. P., Gunalan, S., & Rathinasamy, S. (2024). Green synthesis of zinc oxide nanoparticles using aqueous extract of shilajit and their anticancer activity against HeLa cells. Scientific Reports, 14(1), 2204. https://doi.org/10.1038/S41598-024-52217-X
18. Sheoran, S., Arora, S., Singh, H., Kumar, A., Vuree, S., Vancha, H., & Pawar, S. C. (2023). Characterisation, development and validation of UV Spectrophotometric technique for determining Diosmetin in bulk and nanoformulations. Results in Chemistry, 5, 100972. https://doi.org/10.1016/j.rechem.2023.100972
19. Shiraz, M., Imtiaz, H., Azam, A., & Hayat, S. (2024). Phytogenic nanoparticles: Synthesis, characterization, and their roles in physiology and biochemistry of plants. Biometals, 37(1), 23–70.
20. Steffy, K., Shanthi, G., Maroky, Anson. S., & Selvakumar, S. (2018). Potential bactericidal activity of S. nux-vomica–ZnO nanocomposite against multidrug-resistant bacterial pathogens and wound-healing properties. Journal of Trace Elements in Medicine and Biology, 50, 229–239. https://doi.org/10.1016/j.jtemb.2018.07.009
21. Tayebi-Khorrami, V., Fadaei, M. S., Dabaghi, M. M., Azimi, E., Kalalinia, F., Fadaei, M. R., & Hashemi, M. (2025). Overview of the Application of Nanogels in Wound Healing. Journal of Drug Delivery Science and Technology, 107268.
22. Thien, T. D., Van Thanh, H., Cham, L. T. M., Thang, P. D., Van Thang, N., Van Pham, D., Pham, M. H., Nhat, H. N., Van Hiep, V., & Lam, N. D. (2025). Artificial nano-sized ZnAgO/ZnO/ZnAlO composite material for photocatalytic applications. Heliyon, 11(6), e43029. https://doi.org/10.1016/j.heliyon.2025.e43029
23. Usmaev, B. V., Kagermanov, A. T.-A., Al-Rawashdeh, M. B., Shuaipova, M. M., Bestaeva, K. A., Arshieva, V. A., Guseinova, S. G., & Alieva, K. M. (2024). Investigation of pharmacological and wound-healing properties of zinc oxide nanoparticles. Archives of Pharmacy Practice, 15(4–2024), 10–14.
24. Valipour, F., Rahimabadi, E. Z., & Rostamzad, H. (2023). Preparation and characterization of wound healing hydrogel based on fish skin collagen and chitosan cross-linked by dialdehyde starch. International Journal of Biological Macromolecules, 253, 126704.
25. Xiao, D., Huang, Y., Fang, Z., Liu, D., Wang, Q., Xu, Y., Li, P., & Li, J. (2025). Zinc oxide nanoparticles for skin wound healing: A systematic review from the perspective of disease types. Materials Today Bio, 102221.
26. Yan, Y., Liu, X., Gao, J., Wu, Y., & Li, Y. (2020). Inhibition of TGF-β Signaling in Gliomas by the Flavonoid Diosmetin Isolated from Dracocephalum peregrinum L. Molecules, 25(1), 192. https://doi.org/10.3390/molecules25010192
27. Yusuf, S. N. A. M., Mood, C. N. A. C., Ahmad, N. H., Sandai, D., Lee, C. K., & Lim, V. (2020). Optimization of biogenic synthesis of silver nanoparticles from flavonoid-rich Clinacanthus nutans leaf and stem aqueous extracts. Royal Society Open Science, 7(7), 200065.
28. Zafaryab, M., & Vig, K. (2025). Biomedical application of nanogels: From cancer to wound healing. Molecules, 30(10), 2144.